water

MDPI

Article

Preparation and Modification of Biochar Derived from Agricultural Waste for Metal Adsorption from Urban Wastewater

Maria Cristina Collivignarelli [1,2], W. A. M. A. N. Illankoon [3,*], Chiara Milanese [4], Silvia Calatroni [1], Francesca Maria Caccamo [1], Maria Medina-Llamas [4,5], Alessandro Girella [4] and Sabrina Sorlini [3]

1 Department of Civil Engineering and Architecture, University of Pavia, Via Ferrata 3, 27100 Pavia, Italy; mcristina.collivignarelli@unipv.it (M.C.C.); silvia.calatroni01@universitadipavia.it (S.C.); francescamaria.caccamo01@universitadipavia.it (F.M.C.)
2 Interdepartmental Centre for Water Research, University of Pavia, Via Ferrata 3, 27100 Pavia, Italy
3 Department of Civil, Environmental, Architectural Engineering and Mathematics, University of Brescia, Via Branze 43, 25123 Brescia, Italy; sabrina.sorlini@unibs.it
4 Pavia H2 Lab, Department of Chemistry, Physical Chemistry Section, University of Pavia & C.S.G.I., Viale Taramelli 16, 27100 Pavia, Italy; chiara.milanese@unipv.it (C.M.); maria.medina@uaz.edu.mx (M.M.-L.); alessandro.girella@unipv.it (A.G.)
5 Unidad Académica Preparatoria, Plantel II, Universidad Autónoma de Zacatecas, Zacatecas 98068, Mexico
* Correspondence: a.wijepalaabeysi@unibs.it

Abstract: This work evaluates the efficiency of three biochar samples toward the adsorption of manganese, iron, and selenium present in a sample of urban wastewater. The biochar was produced from the pyrolysis of rice husks at 350 °C for 6 h (RHB) and subsequently modified using HCl (RHB_{HCl}) or NaOH (RHB_{NaOH}) to increase its surface area. The RHB_{NaOH} sample exhibited the highest removal efficiency for the three metals. The metals' adsorption removal efficiency for RHB_{NaOH} was in the order Mn (76%), Se (66%), and Fe (66%), while for RHB_{HCl}, it was Fe (59%), Mn (30%), and Se (26%). The results show that the as-prepared RHB can remove the metals, even if in low amounts (Fe (48%), Mn (3%), and Se (39%)). The adsorption removal for the three types of adsorbents follows the Langmuir isotherm model. Pseudo-first-order and pseudo-second-order models were used to determine the adsorption mechanism for each of the three adsorbents. Both models showed a good fit with R^2 (>0.9) for the RHB_{NaOH} and RHB sorption of Fe, Mn, and Se. Overall, this work demonstrates the potential of biochar for the removal of metals from real wastewater.

Keywords: rice husk; biochar; metal adsorption; urban wastewater; adsorption; wastewater treatment; selenium; manganese; iron

Citation: Collivignarelli, M.C.; Illankoon, W.A.M.A.N.; Milanese, C.; Calatroni, S.; Caccamo, F.M.; Medina-Llamas, M.; Girella, A.; Sorlini, S. Preparation and Modification of Biochar Derived from Agricultural Waste for Metal Adsorption from Urban Wastewater. *Water* **2024**, *16*, 698. https://doi.org/10.3390/w16050698

Academic Editors: Alessandro Erto and Maria Antonia López-Antón

Received: 30 December 2023
Revised: 7 February 2024
Accepted: 24 February 2024
Published: 27 February 2024

1. Introduction

About 71% of the Earth's surface is covered by water, with only 2.5% being fresh water that can be contaminated from a variety of anthropogenic sources, such as municipal, industrial, and agricultural wastewaters [1]. Common pollutants from these sources include heavy metals, pesticides, metalloids, pharmaceuticals, polyaromatic hydrocarbons, and dyes [2]. The consumption of contaminated water is linked to waterborne infections (cholera, diarrhea, and typhoid) and long-term illnesses (cancer and neurodegenerative and endocrine disorders). Currently, more than 2.3 billion people worldwide do not have access to safe drinking water [3].

Metals, such as manganese (Mn), iron (Fe), and selenium (Se), are commonly present in industrial wastewater [4,5]. These elements can be considered as micronutrients for human health [6]. However, concentrations above the recommended daily allowance (RDA) have a detrimental effect on human health. For instance, humans need Mn for enzyme activation, but exposure to values above RDA may induce respiratory illness and neurodegenerative disorders [4,5,7]. Selenium plays a positive role in cancer prevention, but an RDA >

400 μg/day might cause neurodegenerative disorders and dysfunction of the endocrine system [8–10]. Iron is an essential component of hemoglobin and myoglobin, which are responsible for transporting oxygen to the body's tissues and muscles. A long-term exposure to Fe can damage the liver, pancreas, and heart. In addition, the high concentration of Fe in water promotes the development of ferrobacteria, which are linked to odor issues that can generate unpleasant esthetic concerns [4,5]. The World Health Organization (WHO) guidelines for acceptable drinking water concentrations for Mn, Fe, and Se are 0.05, 0.3 mgL^{-1}, and 40 μgL^{-1}, respectively [8–10]. A wide variety of technologies have been developed to remove metals from water. Among them are coagulation–flocculation, membrane filtration, reverse osmosis, chemical precipitation, ion exchange, electrochemical treatment, and flotation [11–16]. These technologies have several drawbacks, such as high energy requirements and high operational and maintenance costs. Moreover, some water treatment technologies are inefficient to remove these pollutants when they are found at low concentrations [17–20]. On the other hand, adsorption is regarded as a popular technology to remove a variety of pollutants from water due to its high efficiency, low cost, and ease of operation [21–24]. It is a technology that can use locally abundant biosorbents, which can reduce operational costs [25,26].

Biochar is a carbon material produced by the thermal decomposition of biomass in an oxygen-free atmosphere [27–33]. It is a highly aromatic compound, made up of layers of graphene and graphite structures and edge carbon atoms containing functional groups, such as carboxylic, hydroxyl, and carbonyl units [33–35]. It is an environmentally friendly adsorbent that can be produced from agricultural, forest, and sewage wastes [36]. Biochar is a relatively inexpensive material because the raw materials are abundant and do not have an economic value. It has been reported that biochar is ~six times cheaper than the most widely used activated carbon [7]. In addition, small pyrolysis reactors can be built with minimal technical requirements and inexpensive materials (e.g., an oil barrel) [32]. Biochar has a porous structure, but the pores are clogged with tarry material produced during the pyrolysis. Consequently, it is usually subjected to a chemical or physical treatment to increase its specific surface area, porosity, and pore size distribution or to incorporate functional groups [37–40]. In a chemical modification process, biochar is treated with strong acids, bases, or chemical oxidants [41]. For instance, biochar obtained from reed samples increased its adsorption capacity toward pentachlorophenol by six-fold when the biochar was treated with 1 M HCl for 6 h [42]. Another report showed NaOH impregnation increased the surface area of wheat straw biochar by 92%, which, in turn, increased by three-fold its adsorption capacity toward toluene [43].

Biochar Adsorption Mechanism

The surface chemistry of modified or unmodified biochar has a strong sorption capacity to remove different types of pollutants from wastewater [37,44,45]. However, the interaction between the adsorbent and adsorbate depends on factors such as the nature of pollutants, pore volume, specific surface area, the hydrophobicity of the adsorbent, and surface functionalization [46]. There are several adsorption mechanisms of biochar toward different organic or inorganic pollutants, such as complexation, precipitation, ion exchange, electrostatic interaction, hydrophobic interaction, pore–filling interaction, and hydrogen bond formation [47,48]. Complexation occurs when oxygen-containing functional groups at the biochar surface interact with the free orbitals of transition metals to form complexes. Precipitation is an important mechanism for the removal of heavy metals, in which the pollutant precipitates either in the solution or over the surface of the biochar. For instance, Pb^{2+} and Cd^{2+} usually precipitate at high pH values as hydroxides. The ion exchange mechanism involves the exchange of ions between the solid (biochar surface) and the liquid interface. Kílıç et al. [49] observed the release of basic metal ions (Ca^{2+}, Na^{+}, and K^{+}) during Hg^{2+} adsorption by an activated sludge biomass, which indicates ion exchange was the adsorption mechanism. Hydrophobic interaction can be described as the attraction between organic compounds (hydrophobic substances) with the layers of graphene of the

biochar. Biochar hydrophobicity increases with the pyrolysis temperature. Consequently, biochar prepared at high temperatures will be efficient for the removal of highly organic pollutants (dyes or pesticides). The pore-filling mechanism depends upon the nature of the biochar and the polarity of the organic contaminant [50]. Pore filling is a process in which the organic contaminants are at the surface of biochar, which has mesopores (2–50 nm) and micropores (<2 nm). Electrostatic interaction is a mechanism based on the attraction and repulsion of charges, which is in essence an ionic bond formation. For instance, cationic pollutants can be adsorbed on the negatively charged surface of biochar [51]. Hydrogen bonds occur due to the intermolecular attraction between the functional groups on the surface of the biochar (-NH_2 or -OH) with organic pollutants that have highly electronegative atoms, such as F, N, or O [40,46,52].

Biochar has shown its potential for the adsorption of metals, such as Pb, Cd, and Cu [53,54]. Little attention has been paid to its adsorption capacity toward Mn or Se. In addition, most of the works reported in the literature were developed using synthetic water. Both factors hinder the potential of biochar to be used as an inexpensive, efficient, and environmentally friendly adsorbent to remove a wide variety of metals from real wastewater. Consequently, in the current work, we prepared a modified biochar from agricultural waste (rice husk). In addition, we evaluated the adsorption capacity of the modified biochar toward three metals (Fe, Mn, and Se) found in a sample of urban wastewater collected from the inlet of a WWTP from Pavia, Italy.

2. Materials and Methods

2.1. Materials

Rice husks were obtained from farmers in the province of Pavia, Lombardy, Italy. All chemical reagents used in this study were of analytical grade from Merck (Kenilworth, NJ, USA). Chemical-grade, 99% pure (SOL S.p.A., Hong Kong, China) nitrogen gas was employed in the pyrolysis process. Deionized (DI) water was used in all preparation and treatment processes.

2.2. Sorbent Materials

2.2.1. Raw Rice Husk (RH)

The rice husk (RH) was washed with DI water to remove impurities coming from the environment and was subsequently dried in an oven at 80 °C overnight. Next, it was ground and sieved using a 1000-micron sieve. Particles lower than 1000 microns were subjected to a ball milling process using a Premium Line P5 planetary mill: 0.4 g of RH was milled in tungsten carbide (WC) jars with 10 WC balls (weight = 1 g/ball), at 500 rpm for 2 cycles with a duration of 60 min/cycle under air atmosphere.

2.2.2. Rice Husk Biochar (RHB)

The ball-milled RH was transferred into an alumina boat and pyrolyzed in a tubular furnace (Carbolite, Sheffield, UK) at 350 °C for 6 h with a heating rate of 10 K/min under N_2 flow (200 mL/min).

2.2.3. Chemically Activated Biochar (RHB_{NaOH})

The pyrolyzed sample (RHB) was activated by soaking the sample in 1 M NaOH (98%, Sigma Aldrich, Burlington, MA, USA) at room temperature for 12 h. We chose NaOH because it is an effective, inexpensive activation agent and is less corrosive than KOH [55–58]. The chosen weight ratio of biochar to NaOH was 2:1. After the alkali treatment, the sample was washed and soaked using 0.1 M HCl (37% *wt*. solution, Sigma Aldrich) under constant agitation until a neutral pH was reached. Next, a vacuum filtration system was used to further wash the sample using DI water. Finally, the NaOH-activated biochar was dried in an oven at 90 °C for 12 h. This sample was labelled as RHB_{NaOH}.

2.2.4. HCl-Treated Rice Husk (RHB_{HCl})

The ball-milled RH was treated with 10% *wt*. HCl for 3 h. After filtration, the solid part was dried at 90 °C in an oven for 20 h and subsequently placed in an oven at 500 °C for 8 h at a heating rate of 10 K/min under N_2 gas flow (200 mL/min). The carbonized sample was cooled up to room temperature under N_2 gas flow and subjected to mild grinding using a mortar and a pestle to obtain a homogeneous powder. This sample was labelled as RHB_{HCl}.

2.3. Characterization

A thermogravimetric analysis (TGA Q5000, TGA Instruments Inc., New Castle, DE, USA) was carried out for all the samples. The measurements were performed using 5 mg of powder by heating from room temperature to 1000 °C at 5 °C/min in an open Pt crucible under N_2 flux. The derivative curve of the mass loss with respect to the temperature (DTG) was obtained by the Universal Analysis V4.5A software provided by TGA Instruments. The FTIR spectra of all the samples were acquired using a Nicolet FTIR iS10 spectrometer (Nicolet, Madison, WI, USA), equipped with aSmart iTR™ Attenuated Total Reflectance (ATR) Sampling Accessory with diamond plate (Nicolet, Madison, WI, USA). Thirty-two scans were collected in a wavenumber range from 4000 cm^{-1} to 600 cm^{-1} with 4 cm^{-1} as the resolution. The surface morphology was analyzed using a scanning electron microscope (Zeiss EvoMA 10 SEM, Oberkochen, Germany) with an acceleration voltage of 20 kV and 8.5 mm as the working distance of the gold-sputtered samples. The EDX analyses were performed on all the samples with an Oxford XMax 50 mm^2 detector coupled with the SEM, following the standard method (ASTM E 1508 [59]). The porosimetry was analyzed by a Sorptomatic 1990 Instrument (ThermoFisher, Waltham, MA, USA) by BET (Brunauer–Emmett–Teller equation) method using N_2 as the adsorption gas. The quantification of Fe, Mn, and Se was performed using inductively coupled plasma optical emission spectroscopy (ICP-OES) (Optima 7000, Perkin Elmer, Waltham, MA, USA), following the standard procedure IRSA-CNR, 3020.

2.4. Testing Conditions

Adsorption batch tests were performed to determine the adsorption efficiency of the modified and unmodified biochar toward Fe, Se, and Mn present in an urban wastewater sample collected at the inlet of a civil wastewater treatment plant (WWTP) located in the province of Pavia (Italy). The sample was a mixture of domestic and industrial wastewater (effluents from agri-food, woodworking, chemical-pharmaceutical, and galvanic factories). The collected urban wastewater was filtrated and kept in a fridge at 4 °C until further use. The initial concentration of the elements obtained by ICP-OES was [Fe] = 0.390 ± 0.103 mg/L, [Mn] = 0.303 ± 0.040 mg/L, and [Se] = 0.116 ± 0.025 mg/L. The pH of the wastewater was 7.6, and it was not modified during the adsorption tests. For the experiments, 0.25 g of biochar was weighed and poured into a flask containing 50 mL of urban wastewater. The liquid sample was kept in agitation at 200 rpm/min at room temperature. Aliquots were taken at different time intervals (0.5, 3, 6, and 9 h). Each aliquot was filtrated with a syringe filter of 22 μm. The residual concentration of each metal was determined using ICP spectroscopy. Each experiment was conducted in duplicate at room temperature. The removal efficiency R (%) was estimated using Equation (1):

$$R(\%) = \frac{(C_0 - C_e)}{C_0} \cdot 100 \quad (1)$$

where C_0 (mg L^{-1}) and C_e (mg L^{-1}) are the initial and equilibrium concentration of the metal, respectively. The adsorption capacity can be calculated using the mass balance shown in Equation (2):

$$Q_e = (C_0 - C_e) \times \frac{V}{M} \quad (2)$$

where V represents the total volume of the solution (L) and M is the mass of the adsorbent (g).

2.5. Adsorption Kinetics

Pseudo-first-order and pseudo-second-order kinetic equations [60–62] were used to approximate the adsorption rate and mechanism. Equation (3) represents a pseudo-first-order model.

$$ln(Q_e - Q_t) = lnQ_e - k_1 t \quad (3)$$

where k_1 is the equilibrium rate constant of the pseudo-first-order model (h^{-1}). The slope and intercept of the linear graph $ln\ (Q_e - Q_t)$ vs. t were used to determine k_1 and Q_e, respectively. Equation (4) is a pseudo-second-order model that encompasses all adsorption processes, including external film diffusion, adsorption, and internal particle diffusion.

$$\frac{t}{Q_t} = \frac{1}{k_2 {Q_e}^2} + \frac{t}{Q_e} \quad (4)$$

The pseudo-second-order adsorption model defines Q_e and Q_t as the adsorption capacities of the adsorbent at equilibrium and at time t (h), respectively. k_2 is the rate constant the pseudo-second-order model (g/mg h). Q_e and k_2 can be calculated, respectively, from the slope and intercept of the linear plot of t/Q_t vs. t.

2.6. Adsorption Isotherm

The adsorption capacity of heavy metals onto the adsorbent can be evaluated using the two most widely used equations: the Langmuir and Freundlich isotherms. The Langmuir isotherm, a basic model for the adsorption equilibrium, is applicable over a wide range of pressures. The Langmuir equation describes some assumptions governing the coverage of adsorbate molecules on solid surfaces as a function of the partial pressure or concentration at a constant temperature [63–65]:

1. Adsorption occurs at several active sites on the surface.
2. Each active site attracts only a single molecule.
3. The adsorbing surface is fairly homogeneous.
4. There are no interactions between the adsorbed molecules.

The first one, the Langmuir model, indicates a monolayer adsorption mechanism, with a finite number of adsorption sites on a homogeneous surface. When an adsorbent is entirely covered by a monolayer, its maximum capacity can be calculated using the Langmuir isotherm model. The equation for the Langmuir isotherm is shown below (Equation (5)) [63–65]:

$$\frac{C_e}{Q_e} = \frac{1}{K_L Q_m} + \frac{C_e}{Q_m} \quad (5)$$

Q_m is the maximum adsorption capacity of the adsorbent material in terms of mg/g, and K_L is the Langmuir constant (L/mg), which is correlated to the adsorption energy relation. The values of Q_m and K_L are determined by the linear plot of C_e/Q_e versus C_e as the slope and intercept, respectively. According to Webber and Chakraborty's definition [66,67], the efficiency of the adsorption process could be predicted by the dimensionless parameter R_L (Equation (6)):

$$R_L = \frac{1}{1 + K_L C_0} \quad (6)$$

where C_0 is the metal concentration at time zero (mg/L). If $R_L = 0$, the adsorption process is considered irreversible. An R_L value ($0 < R_L < 1$) indicates favorable adsorption, while a value of $R_L > 1$ represents an unfavorable adsorption. However, in this experimental work, there was favorable adsorption because all R_L values for all metals were found to be between 0 and 1.

In contrast to Langmuir isomerization, multilayer adsorption at heterogeneous sites can be performed using the Freundlich empirical model [68]. The Freundlich isotherm explains multilayer adsorption and expects the energy distribution of adsorbed sites to

drop exponentially [68,69]. The Freundlich adsorption isotherm model is shown below (Equation (7)) [68–70].

$$\ln Q_e = \ln K_F + \frac{1}{n} \ln C_e \quad (7)$$

where K_F and n are constants related to the adsorption capacity of the material and the intensity of the adsorption, respectively. Both values can be calculated from the slope and intercept of the plot between $\ln Q_e$ vs. $\ln C_e$. When $1/n$ lies between 0 and 1, the adsorption is considered favorable. On the other hand, an unfavorable adsorption happens when $n = 0$ and the adsorption process is irreversible; when $n < 1$, the process is favorable; when $n = 1$, the process is linear; and when $n > 1$, the adsorption process is unfavorable [67,71]. The Freundlich equation, which provides information on particle sorption, has numerous limitations [71,72]:

1. It is simply empirical, with no theoretical foundation.
2. Validity is confined to a fixed concentration range; beyond that point, nonlinearity arises.
3. The constant K might fluctuate as the temperature varies.

However, it resulted not valid for some adsorption data [71,72].

3. Results and Discussion

3.1. Characterization of the Biochar

Figure 1 shows the TGA and DTG curves for the RH, RHB, RHB_{NaOH}, and RHB_{HCl} samples. For the raw RH, the graph shows four mass loss stages. The first one accounts for 8.4% mass loss with respect to the total weight and takes place between 100 °C and 150 °C, and is originated by moisture content. During the second mass loss, between 150 °C and 250 °C, 18.1% of the mass loss occurs due to the degradation of hemicellulose and the initial decomposition of lignin. This biomass component begins to decompose at around 160 °C, but the process is sluggish, and the decomposition continues until the temperature reaches 900 °C [73]. The third stage of weight loss (48.9%) occurs from 250 °C to 400 °C and is due to the degradation of lignin and cellulose [73–75]. The DTG curve shows the highest degradation rate in this temperature range. The fourth step (400 °C–1000 °C) accounts for 11.9% *wt* of mass loss and occurs due to the continuous elimination of different types of carbonaceous components [75–77]. The obtained TGA profile of the RH is similar to those found in the literature for RHs [78,79]. The TGAs for the RHB (Figure 1b), RHB_{NaOH} (Figure 1c), and RHB_{HCl} (Figure 1d) samples are quite similar. The plots show a first mass loss around 100 °C, due to the elimination of water. For RHB and RHB_{NaOH}, a second mass loss centered at 500 °C indicates the elimination of the remaining volatile organic mass. This peak shifts toward higher temperatures for the RHB_{HCl} sample because this sample was subjected to a second heat treatment after HCl impregnation, which already allowed for the degradation of a larger organic component amount with respect to the other samples. Finally, RHB, RHB_{NaOH}, and RHB_{HCl} had a third mass loss peak starting at 800 °C, which corresponds to the additional elimination of various carbonaceous components [75–77].

Figure 2 shows the FTIR spectra acquired from all the samples. First, the RH spectrum shows a broad peak at 3440 cm^{-1} due to the O-H stretching vibration of the water molecules adsorbed on the sample. The former peak is barely visible for the RHB and the RHB_{NaOH} samples, which were thermally treated after the chemical treatments. The bands for RHB, RHB_{NaOH}, and RHB_{HCl} are oversimplified, owing to the elimination of several functional groups during the pyrolysis steps [33,80]. The RH sample shows a weak peak at 2929 cm^{-1} due to the methylene group -CH_2- in hemicellulose and cellulose. This peak disappears for the RHB due to the pyrolysis step at 350 °C. The RH, RHB, and RHB_{NaOH} have a couple of weak bands between 2000 cm^{-1} and 2500 cm^{-1} that correspond to the vibrations of C≡C and C≡N. For the RH, RHB, and RHB_{NaOH} samples, there is a peak at 1653 cm^{-1} that denotes the presence of C=C bonds from lignin and cellulose. The peak at around 1630 cm^{-1} indicates the presence of N-H bonds in RRH, RHB, and RHB_{NaOH}. Both peaks are absent in the RHB_{HCl}. The peaks between 1500 cm^{-1} and 1100 cm^{-1} reflect the presence of carbonate and carbonate-carboxyl groups in RHB_{HCl}. In the RH, the peaks around

1153–1300 cm^{-1} indicate the C-O stretching from an ester or phenol: they are almost vanished in the pyrolyzed and chemically treated samples. For the RH, the signals at 1080, 898, 796, and 662 cm^{-1} can be attributed to the stretching vibrations of the siloxane groups [78]. RHB_{HCl} has a prominent peak at 1051 cm^{-1} attributed to the siloxane (Si-O-Si) network vibration modes, indicating a highly condensed silica network [81]. The former peak is clearly visible in RHB_{HCl}, as reported in the literature [82]. The signal at 794 cm^{-1} indicates the aromatic C-H out-of-plane bend [83]. The former peaks have a lower intensity in the pyrolyzed sample.

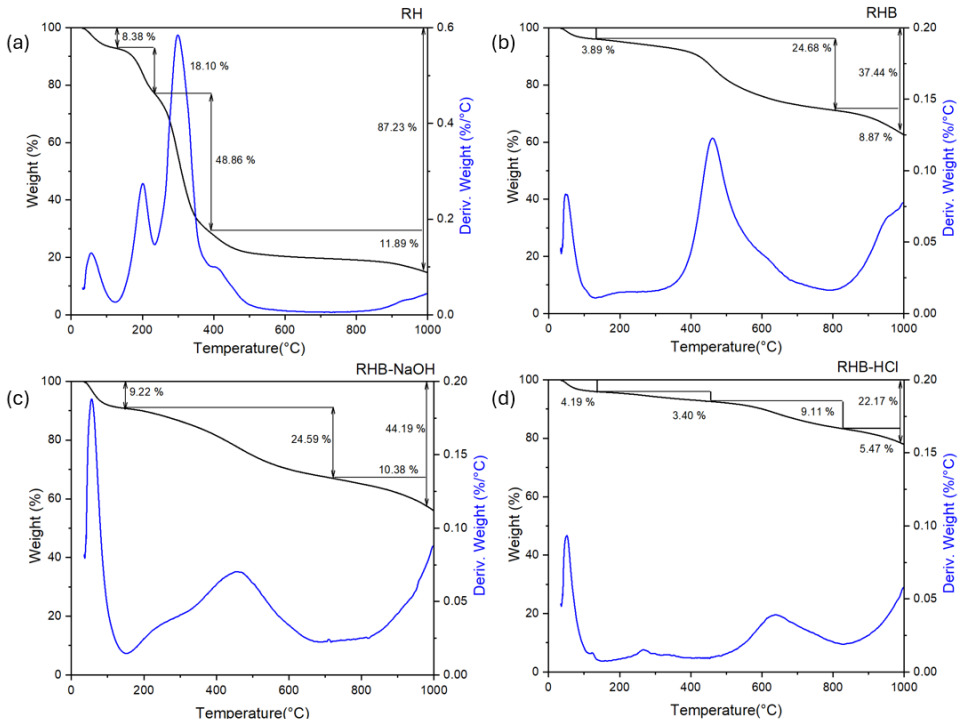

Figure 1. TGA (black line) and DTG (blue line) curves for the (**a**) rice husk (RH), (**b**) rice husk biochar (RHB), and the (**c**) NaOH- and (**d**) HCl-activated biochar samples.

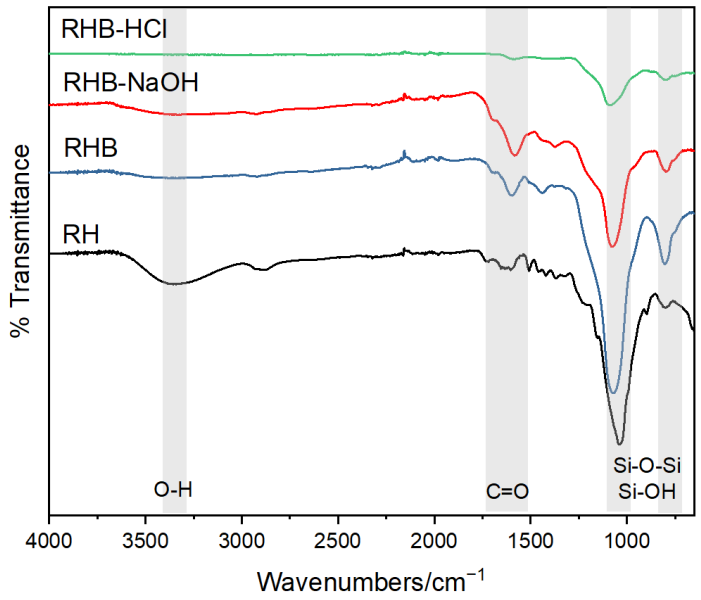

Figure 2. FTIR analysis of the rice husk (RH), rice husk biochar (RHB), and NaOH- and HCl-activated biochar samples.

Table 1 shows the elemental analysis obtained for all the samples by EDX. For the RH, carbon, oxygen, and silicon are the main constituents, with Si and O being probably present in the form of silica. The chemical composition of the RH differs after the pyrolysis and the chemical modifications. Using EDX, H and N cannot be detected. After pyrolysis (RHB), C becomes the main component due to the decomposition of lignin, cellulose, and hemicellulose [33,84]. The end products of pyrolysis are biochar, bio-oil, and syngas (CO, CO_2, CH_4, and H_2), and the amount of each product is determined by the pyrolysis temperature, heat flux, N_2 flow rate, and residence time [84–86]. The stability of biochar is increased by the removal of different components in gaseous and volatile forms, which results in a reduction in the O/C and H/C atomic ratios and the corresponding rise in aromaticity and the carbon content [87,88].

Table 1. Elemental composition obtained by SEM-EDX of the rice husk (RH), rice husk biochar (RHB), and NaOH- and HCl-activated biochar samples.

Element	% Weight			
	RH	RHB	RHB-HCl	RH-NaOH
C	39.34	54.97	61.99	61.69
O	47.30	34.08	26.10	30.97
Si	13.36	10.52	11.91	5.46
Ca	-	0.29	-	0.33
S	-	0.14	-	0.11
Na	-	-	-	1.44

Figure 3 shows the SEM images of all the samples. The RH shows micro-sized fragments with a wavy structure. The pyrolysis step clearly reduces the size of the fragments. The specific surface area of the RHB is 52 m^2/g. The SEM micrograph of RHB_{NaOH} shows a smooth surface. The surface area of RHB_{NaOH} is 360 m^2/g. This clearly indicates that NaOH activation leads to the formation of porosity. RHB_{HCl} has a smooth morphology and achieves a surface area of 280 m^2/g. The pores can act as highways for ion diffusion. Additionally, the presence of pores increases the ratio between the surface area and volume and its effect on the overall specific surface area [33,89].

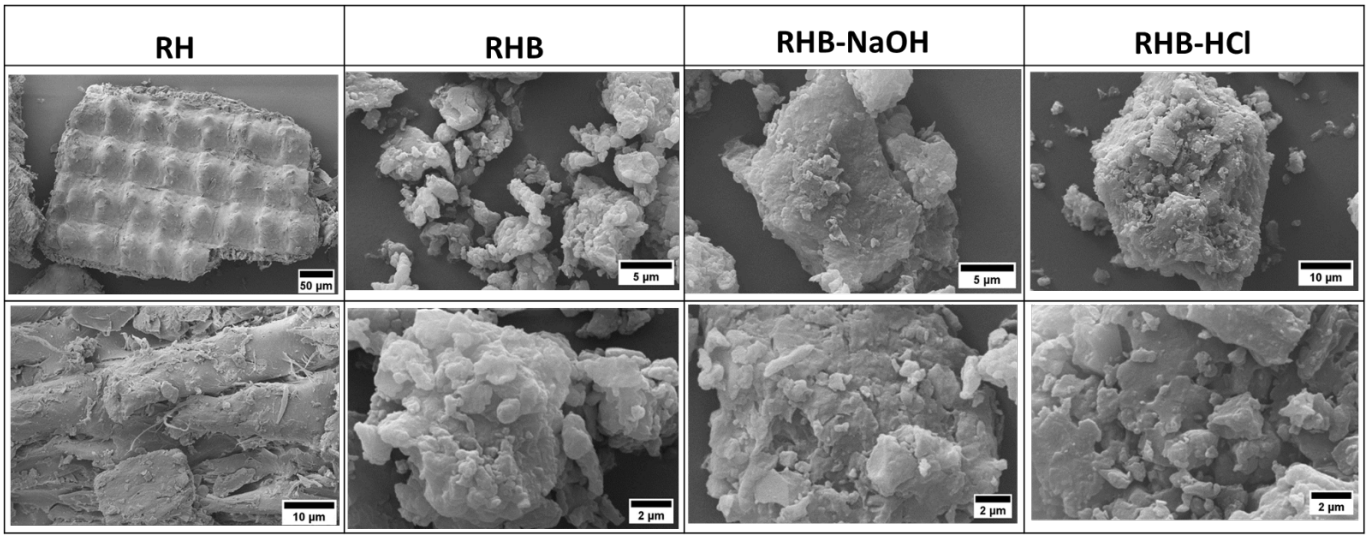

Figure 3. SEM morphology analysis of the rice husk (RH), rice husk biochar (RHB), and NaOH- and HCl-activated biochar samples.

3.2. Removal of Metals

Urban wastewater contains a wide variety of organic and inorganic pollutants. These contaminants may include dyes, heavy metals, surfactants, medicines, pesticides, or per-

sonal care products. Reports in the literature have demonstrated that various types of biomasses have an outstanding capacity to remove contaminants from wastewater [90]. It is commonly acknowledged that the adsorption capability of metals toward biochar is primarily determined by the feedstock properties, pyrolysis temperature, residence time, and the nature of the target metals.

In this work, the preliminary analysis of an urban wastewater sample, collected at the inlet of a wastewater treatment plant, showed the presence of various elements, such as As, B, Ba, Cd, Cr, Fe, Mn, Ni, Pb, Zn, Se, and Sn. However, we evaluated the adsorption capacity of biochar samples toward Fe, Mn, and Se.

Iron (Fe), Manganese (Mn), and Selenium (Se) Removal

Adsorption batch tests were performed to determine the removal efficiency of RHB, RHB_{NaOH}, and RHB_{HCl} toward Fe, Se, and Mn, present in an urban wastewater sample collected from a civil wastewater treatment plant (WWTP) located in the province of Pavia, Italy. The samples were collected at the WWTP inlet. The pH of the urban wastewater was 7.6, and it was not modified to perform the adsorption experiments.

Figure 4 shows the percentage of metal adsorbed as a function of the interaction time for each metal and for the three biochar samples (RHB, RHB_{NaOH}, and RHB_{HCl}). The results show, in all the cases, a positive correlation between the adsorption removal and the interaction time. The RHB_{NaOH} sample has the highest affinity toward Fe, Mn, and Se, as it is able to absorb up to 66%, 76%, and 66% after 6 h of interaction time, respectively. The RHB_{HCl} sample is able to absorb 59% Fe, 30% Mn, and 26% Se after 6 h of interaction time. RHB is able to adsorb 48% Fe and 40% Se. However, RHB does not show affinity toward Mn, adsorbing only 2.75%. Table 2 shows the initial concentration (C_0) and equilibrium concentration (C_e) of each metal after 9 h of interaction time.

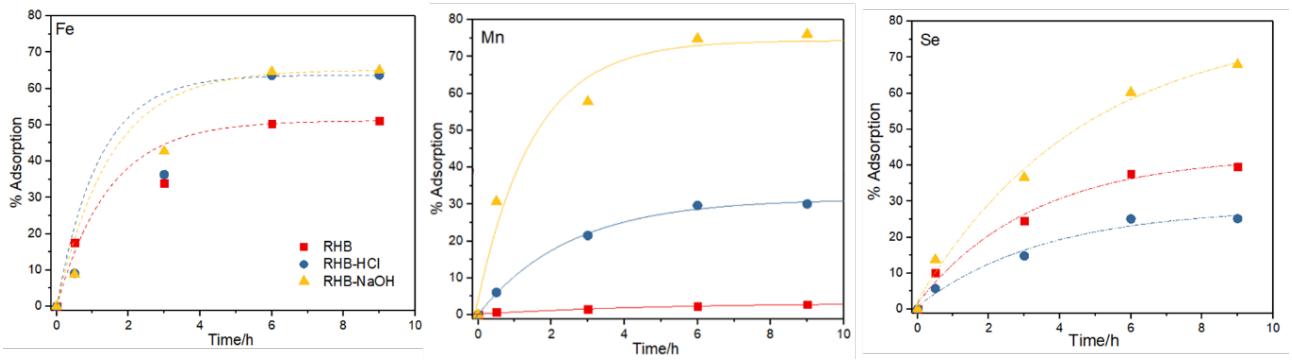

Figure 4. Adsorption removal efficiency (% *R*) against time for each metal by the rice husk (RH), rice husk biochar (RHB), and NaOH- and HCl-activated biochar samples.

Table 2. Initial concentration (C_0) of Fe, Mn, and Se collected from urban wastewater and the equilibrium concentration (C_e) after the adsorption experiments. Experimental conditions: 0.25 g biochar and 50 mL urban wastewater under agitation at 200 rpm for 9 h.

Type of Biochar	Initial Concentration C_0 (mg/L)		
	Fe	**Mn**	**Se**
	0.39 ± 0.103	**0.303 ± 0.04**	**0.116 ± 0.025**
	Equilibrium Concentration C_e (mg/L)		
RHB_{NaOH}	0.133 ± 0.040	0.073 ± 0.018	0.039 ± 0.015
RHB_{HCl}	0.160 ± 0.053	0.212 ± 0.034	0.086 ± 0.020
RHB	0.204 ± 0.063	0.294 ± 0.040	0.070 ± 0.016

3.3. Removal Mechanisms

The adsorption capacity of an adsorbent strongly depends on the properties of the adsorbent, such as the ionic radius, surface area, electronegativity, and the surface's functional groups [91]. Other factors that should be considered are the pH or temperature of the water. For instance, at pH 7.6, Mn should be present in water as a small cation, Mn^{+2}. The possible adsorption mechanism is due to electrostatic interactions between Mn^{+2} and negatively charged functional groups, such as hydroxyl, carboxyl, and carbonyl, on the surface of the biochar [91]. At a neutral pH, iron is mainly in the two forms of Fe^{2+} or $Fe(OH)_3$ [92]. We believe that the high adsorption values toward Fe using the three adsorbents must be a combination of the two mechanisms. The first one is the electrostatic interaction between Fe^{+2} and negatively charged functional groups, as described above. The second mechanism is a complexation mechanism due to the high amount of OH- groups from the RHB_{NaOH} [93]. Under the tested experimental conditions (pH 7.6), selenium is in the form of $HSeO_3^-$ and SeO_4^{-2} [94]. It has been reported in the literature that negatively charged selenate groups can be adsorbent on the surface of biochar due to the presence of metallic cations, such as Na^{+1} and Ca^{+2} (as reported in the SEM-EDX analysis).

We would like to highlight that the best-performing material toward the three metals was the biochar modified with NaOH. On the other hand, RHB and RHB_{HCl} had a relatively poor performance toward the adsorption of Se.

3.4. Effect of the Contact Time on Fe, Mn, and Se Removal

Table 3 displays the correlation between the contact time of municipal wastewater samples and the removal of Fe, Mn, and Se for each kind of biochar. For the same contaminants, the equilibrium contact period for RHB_{NaOH} and RHB adsorbents are quite close. Nonetheless, RHB_{HCl} does not exhibit the same properties as the other two adsorbents. The efficiency of the sorbents in removing Fe, Mn, and Se was measured using pseudo-first order (Equation (3)) and pseudo-second-order (Equation (4)) models. When compared to the other two adsorbents, RHB_{NaOH} is more effective in removing the metals Fe, Mn, and Se (Figure 4).

Table 3. Adsorption kinetic modeling for Fe, Mn, and Se adsorption by the biochar materials.

Types of Adsorbents	Fe						Mn						Se					
	First Order			Second Order			First Order			Second Order			First Order			Second Order		
	Q_e	K_1	R^2	Q_e	K_2	R^2	Q_e	K_1	R^2	Q_e	K_2	R^2	Q_e	K_1	R^2	Q_e	K_2	R^2
RHB_{NaOH}	0.391	2.250	0.941	0.077	3.474	0.951	0.507	2.998	0.945	0.051	18.997	0.995	0.745	4.366	0.998	0.020	28.769	0.983
RHB_{HCl}	1.838	4.381	0.593	0.070	4.542	0.886	0.479	3.567	0.947	0.024	20.950	0.989	0.534	4.161	0.900	0.007	39.873	0.248
RHB	0.485	2.891	0.922	0.048	13.996	0.985	0.751	6.438	0.968	0.002	144.308	0.933	0.593	4.500	0.939	0.012	35.669	0.975

In addition, the adsorption of Fe, Mn, and Se by RHB_{NaOH} and RHB fits the pseudo-second-order model ($R^2 > 0.98$) well. Pseudo-first- and pseudo-second-order model plots were used to determine Q_e values for all adsorbents. The Q_e values from the pseudo-second-order model were very similar to the experimental data (calculated using Equation (2) and displayed in Table 4). These results indicate that the adsorption of the three metals follows a chemisorption mechanism. Previous works have reported that metal adsorption by biomass follows a pseudo-second-order model: sunflower [95], paper mill sludge [96], oyster shell waste [97], apple tree branches [98], chicken manure [99], and rice husk [60] were used as adsorbents. Consequently, electrostatic attraction, ion exchange, complexation, and precipitation among the active sites of the adsorbent all contribute to the sorption of the three metals Fe, Mn, and Se (Figure 5).

Table 4. Adsorption efficiency (% *R*) and adsorption capacity (Q_e). Experimental conditions: 0.25 g biochar and 50 mL urban wastewater under agitation at 200 rpm for 9 h.

Type of Biochar	Fe		Mn		Se	
	% *R*	Q_e (mg/g)	% *R*	Q_e (mg/g)	% *R*	Q_e (mg/g)
RHB_{NaOH}	65.98	0.05	75.77	0.05	66.28	0.02
RHB_{HCl}	58.97	0.05	29.85	0.02	25.94	0.01
RHB	47.61	0.04	2.75	0.00	39.48	0.01

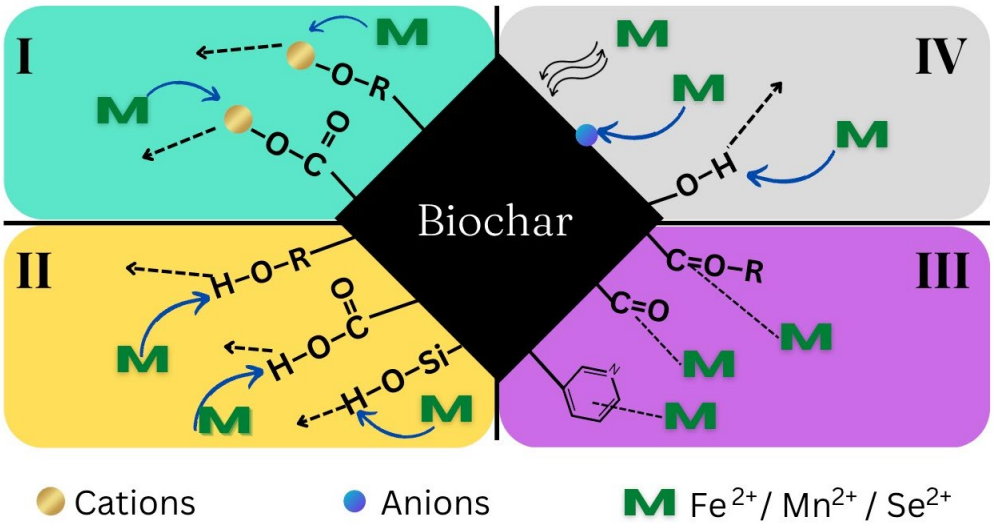

Figure 5. Mechanisms of metal removal using the synthesized biochar (**I**: ion exchange; **II**: surface complexation; **III**: p-electron interactions; and **IV**: physical adsorption, co-precipitation, and surface precipitation).

3.5. Isotherm Analysis of RHB_{NaOH}, RHB_{HCl}, and RHB

To describe the adsorption behavior, the experimental data were fitted using the Langmuir and Freundlich models. Both models are widely used for metal adsorption processes. Table 3 displays the results of adsorption isotherm modelling for the three materials for Fe, Mn, and Se. The Langmuir monolayer isotherm provides the best fit, which is in line with previous research employing biochar for metal removal using biomass and biochar samples [60,100,101]. The Langmuir model indicates a monolayer adsorption mechanism, with a finite number of adsorption sites on a homogeneous surface. The adsorption efficiency is quantified using the R_L value, which is a dimensionless constant separation factor. To determine this, it compares the entire adsorbent capacity to the total adsorbent capacity that was not used. If the R_L value falls between 0 and 1, it indicates a favorable adsorption [60,102]. Table 5 shows the R_L for all samples. Fe adsorption by RHB_{NaOH} has the highest R_L value of 0.486. The calculated Q_{max} values of 0.198 mg/g for Fe sorption by RHB_{NaOH}, 0.088 mg/g for Fe sorption by RHB, and 0.077 mg/g for Mn sorption were measured for all samples using the urban wastewater. The Q_{max} values for Mn sorption by RHB were as low as 0.002 mg/g. These adsorbents had Q_{max} values consistent with those reported in previous reports in the literature using chitosan biochar to treat industrial wastewater [103].

Table 5. Adsorption isotherm modeling for Fe, Mn, and Se adsorption by the biochar materials.

Types of Adsorbents	Fe						Mn						Se					
	Langmuir			Freundlich			Langmuir			Freundlich			Langmuir			Freundlich		
	Q_{max} (mg/g)	R_L	R^2	K_F (mg/g)	n	R^2	Q_{max} (mg/g)	R_L	R^2	K_F (mg/g)	n	R^2	Q_{max} (mg/g)	R_L	R^2	K_F (mg/g)	n	R^2
RHB_{NaOH}	0.198	0.486	0.904	0.247	1.296	0.999	0.077	0.140	0.859	0.119	2.743	0.646	0.022	0.135	0.677	0.030	4.857	0.100
RHB_{HCl}	0.071	0.198	0.464	0.120	1.877	0.304	0.032	0.350	0.668	0.035	2.386	0.464	0.011	0.411	0.960	0.031	1.509	0.995
RHB	0.088	0.415	0.527	0.109	1.484	0.769	0.002	0.075	0.140	0.002	8.850	0.005	0.009	0.016	0.851	0.089	1.169	0.993

Considering Langmuir adsorption isotherm modelling, the RHB_{NaOH} sorbent has a significant capacity of 0.297 mg/g for metal ion adsorption for varying concentrations of mixed metal ions wastewater samples. Similarly, the RHB_{HCl} sorbent has a substantial adsorption capability of 0.213 mg/g, but the RHB sorbent has a relatively lower capacity of 0.099 mg/g. These findings also highlight the significance of evaluating the sorbent performance, rather than making direct comparisons of the metal ion removal efficiency.

4. Conclusions

In this work, we produced a biochar by pyrolysis from rice husks and we treated it with NaOH or HCl to increase its surface area. The three materials were tested for the adsorption of Fe, Mn, and Se present in an urban wastewater sample collected from the inlet of a wastewater facility in Pavia, Italy. The results indicate that the best adsorbent toward the three metals (Fe, Mn, and Se) is RHB_{NaOH} due to the high surface area (360 m^2/g) and the presence of functional groups. The adsorption kinetics had a good fit using the pseudo-second-order model, while the Langmuir monolayer isotherm described the adsorption behavior of the three metals. The maximum adsorption capacities for Fe, Mn, and Se were found at 0.05, 0.05, and 0.02 mg/g RHB_{NaOH}, respectively. The adsorption mechanisms for the three metals were surface complexation and electrostatic interactions. This work provides an insight into the use of modified biochar for the removal of metals from real wastewater. Further studies will optimize the materials and explore their practical applicability to wastewater treatment plants.

Author Contributions: Conceptualization, M.C.C., C.M. and S.S.; methodology, M.C.C., W.A.M.A.N.I., C.M. and S.S.; software, W.A.M.A.N.I. and S.C.; validation, W.A.M.A.N.I., C.M. and S.C.; formal analysis, W.A.M.A.N.I., S.C., F.M.C., M.M.-L. and A.G.; investigation, W.A.M.A.N.I., S.C. and F.M.C.; data curation, W.A.M.A.N.I., M.M.-L. and S.C.; writing—original draft preparation, W.A.M.A.N.I.; writing—review and editing, M.C.C., W.A.M.A.N.I., C.M., M.M.-L. and S.S.; supervision, C.M., M.C.C. and S.S. All authors have read and agreed to the published version of the manuscript.

Funding: This research received no external funding.

Data Availability Statement: The data presented in this study are available upon request from the corresponding author.

Acknowledgments: The authors thank Azienda Agricola Cascina Alberona (Mortara, PV, Italy), Azienda Agricola Cassi Cugini (Sant'Angelo Lomellina, PV, Italy), and Azienda Agricola DICRISTIANA (Robbio, PV, Italy) for supplying the rice husk for the experimental analyses. M.C.C. and C.M. acknowledge support from the Ministero dell'Università e della Ricerca (MUR) and the University of Pavia through the program "Dipartimenti di Eccellenza 2023–2027".

Conflicts of Interest: The authors declare no conflicts of interest.

References

1. Rajasulochana, P.; Preethy, V. Comparison on Efficiency of Various Techniques in Treatment of Waste and Sewage Water—A Comprehensive Review. *Resour.-Effic. Technol.* **2016**, *2*, 175–184. [CrossRef]
2. Medina-Llamas, M.; Taylor, C.M.; Ji, J.; Wenk, J.; Mattia, D. Continuous Production of Metal Oxide Nanoparticles via Membrane Emulsification–Precipitation. *Ind. Eng. Chem. Res.* **2020**, *59*, 9085–9094. [CrossRef]
3. Li, X.; Wang, C.; Zhang, J.; Liu, J.; Liu, B.; Chen, G. Preparation and Application of Magnetic Biochar in Water Treatment: A Critical Review. *Sci. Total Environ.* **2020**, *711*, 134847. [CrossRef]

4. Elsehly, E.M.I.; Chechenin, N.G.; Bukunov, K.A.; Makunin, A.V.; Priselkova, A.B.; Vorobyeva, E.A.; Motaweh, H.A. Removal of Iron and Manganese from Aqueous Solutions Using Carbon Nanotube Filters. *Water Supply* **2016**, *16*, 347–353. [CrossRef]
5. Kim, H.; Ko, R.-A.; Lee, S.; Chon, K. Removal Efficiencies of Manganese and Iron Using Pristine and Phosphoric Acid Pre-Treated Biochars Made from Banana Peels. *Water* **2020**, *12*, 1173. [CrossRef]
6. Nieder, R.; Benbi, D.K.; Reichl, F.X. Microelements and Their Role in Human Health. In *Soil Components and Human Health*; Springer Netherlands: Berlin/Heidelberg, Germany, 2018; pp. 317–374.
7. Idrees, M.; Batool, S.; Ullah, H.; Hussain, Q.; Al-Wabel, M.I.; Ahmad, M.; Hussain, A.; Riaz, M.; Ok, Y.S.; Kong, J. Adsorption and Thermodynamic Mechanisms of Manganese Removal from Aqueous Media by Biowaste-Derived Biochars. *J. Mol. Liq.* **2018**, *266*, 373–380. [CrossRef]
8. Lee, N.; Hong, S.-H.; Lee, C.-G.; Park, S.-J.; Lee, J. Conversion of Cattle Manure into Functional Material to Remove Selenate from Wastewater. *Chemosphere* **2021**, *278*, 130398. [CrossRef] [PubMed]
9. Hansen, H.K.; Peña, S.F.; Gutiérrez, C.; Lazo, A.; Lazo, P.; Ottosen, L.M. Selenium Removal from Petroleum Refinery Wastewater Using an Electrocoagulation Technique. *J. Hazard. Mater.* **2019**, *364*, 78–81. [CrossRef] [PubMed]
10. Gebreeyessus, G.D.; Zewge, F. A Review on Environmental Selenium Issues. *SN Appl. Sci.* **2019**, *1*, 55. [CrossRef]
11. Ramirez-Canon, A.; Medina-Llamas, M.; Vezzoli, M.; Mattia, D. Multiscale Design of ZnO Nanostructured Photocatalysts. *Phys. Chem. Chem. Phys.* **2018**, *20*, 6648–6656. [CrossRef]
12. Nharingo, T.; Moyo, M. Application of Opuntia Ficus-Indica in Bioremediation of Wastewaters. A Critical Review. *J. Environ. Manag.* **2016**, *166*, 55–72. [CrossRef]
13. Ejraei, A.; Aroon, M.A.; Ziarati Saravani, A. Wastewater Treatment Using a Hybrid System Combining Adsorption, Photocatalytic Degradation and Membrane Filtration Processes. *J. Water Process Eng.* **2019**, *28*, 45–53. [CrossRef]
14. Guillossou, R.; Le Roux, J.; Mailler, R.; Pereira-Derome, C.S.; Varrault, G.; Bressy, A.; Vulliet, E.; Morlay, C.; Nauleau, F.; Rocher, V.; et al. Influence of Dissolved Organic Matter on the Removal of 12 Organic Micropollutants from Wastewater Effluent by Powdered Activated Carbon Adsorption. *Water Res.* **2020**, *172*, 115487. [CrossRef]
15. Vunain, E.; Masoamphambe, E.F.; Mpeketula, P.M.G.; Monjerezi, M.; Etale, A. Evaluation of Coagulating Efficiency and Water Borne Pathogens Reduction Capacity of Moringa Oleifera Seed Powder for Treatment of Domestic Wastewater from Zomba, Malawi. *J. Environ. Chem. Eng.* **2019**, *7*, 103118. [CrossRef]
16. Maleki, A.; Mahvi, A.H.; Zazouli, M.A.; Izanloo, H.; Barati, A.H. Aqueous Cadmium Removal by Adsorption on Barley Hull and Barley Hull Ash. *Asian J. Chem.* **2011**, *23*, 1373–1376.
17. Cheng, Z.; Fu, F.; Dionysiou, D.D.; Tang, B. Adsorption, Oxidation, and Reduction Behavior of Arsenic in the Removal of Aqueous As(III) by Mesoporous Fe/Al Bimetallic Particles. *Water Res.* **2016**, *96*, 22–31. [CrossRef] [PubMed]
18. He, J.; Li, Y.; Cai, X.; Chen, K.; Zheng, H.; Wang, C.; Zhang, K.; Lin, D.; Kong, L.; Liu, J. Study on the Removal of Organic Micropollutants from Aqueous and Ethanol Solutions by HAP Membranes with Tunable Hydrophilicity and Hydrophobicity. *Chemosphere* **2017**, *174*, 380–389. [CrossRef]
19. Fu, F.; Wang, Q. Removal of Heavy Metal Ions from Wastewaters: A Review. *J. Environ. Manag.* **2011**, *92*, 407–418. [CrossRef]
20. Ehrampoush, M.H.; Miria, M.; Salmani, M.H.; Mahvi, A.H. Cadmium Removal from Aqueous Solution by Green Synthesis Iron Oxide Nanoparticles with Tangerine Peel Extract. *J. Environ. Health Sci. Eng.* **2015**, *13*, 84. [CrossRef]
21. Xu, Y.; Chen, J.; Chen, R.; Yu, P.; Guo, S.; Wang, X. Adsorption and Reduction of Chromium(VI) from Aqueous Solution Using Polypyrrole/Calcium Rectorite Composite Adsorbent. *Water Res.* **2019**, *160*, 148–157. [CrossRef]
22. Khataee, A.R.; Kasiri, M.B. Photocatalytic Degradation of Organic Dyes in the Presence of Nanostructured Titanium Dioxide: Influence of the Chemical Structure of Dyes. *J. Mol. Catal. A Chem.* **2010**, *328*, 8–26. [CrossRef]
23. Haddad, M.Y.; Alharbi, H.F. Enhancement of Heavy Metal Ion Adsorption Using Electrospun Polyacrylonitrile Nanofibers Loaded with ZnO Nanoparticles. *J. Appl. Polym. Sci.* **2019**, *136*, 47209. [CrossRef]
24. Haddad, M.; Oie, C.; Vo Duy, S.; Sauvé, S.; Barbeau, B. Adsorption of Micropollutants Present in Surface Waters onto Polymeric Resins: Impact of Resin Type and Water Matrix on Performance. *Sci. Total Environ.* **2019**, *660*, 1449–1458. [CrossRef]
25. Mahvi, A.H. Application of Agricultural Fibers in Pollution Removal from Aqueous Solution. *Int. J. Environ. Sci. Technol.* **2008**, *5*, 275–285. [CrossRef]
26. Dehghani, M.H.; Mahvi, A.H.; Rastkari, N.; Saeedi, R.; Nazmara, S.; Iravani, E. Adsorption of Bisphenol A (BPA) from Aqueous Solutions by Carbon Nanotubes: Kinetic and Equilibrium Studies. *Desalination Water Treat.* **2015**, *54*, 84–92. [CrossRef]
27. Yuan, Y.; Chesnutt, B.M.; Haggard, W.O.; Bumgardner, J.D. Deacetylation of Chitosan: Material Characterization and in Vitro Evaluation via Albumin Adsorption and Pre-Osteoblastic Cell Cultures. *Materials* **2011**, *4*, 1399–1416. [CrossRef]
28. Regmi, P.; Garcia Moscoso, J.L.; Kumar, S.; Cao, X.; Mao, J.; Schafran, G. Removal of Copper and Cadmium from Aqueous Solution Using Switchgrass Biochar Produced via Hydrothermal Carbonization Process. *J. Environ. Manag.* **2012**, *109*, 61–69. [CrossRef]
29. Beesley, L.; Marmiroli, M. The Immobilisation and Retention of Soluble Arsenic, Cadmium and Zinc by Biochar. *Environ. Pollut.* **2011**, *159*, 474–480. [CrossRef] [PubMed]
30. Illankoon, W.A.M.A.N.; Milanese, C.; Collivignarelli, M.C.; Sorlini, S. Value Chain Analysis of Rice Industry by Products in a Circular Economy Context: A Review. *Waste* **2023**, *1*, 333–369. [CrossRef]
31. Collivignarelli, M.C.; Sorlini, S.; Milanese, C.; Illankoon, W.A.M.A.N.; Caccamo, F.M.; Calatroni, S. Rice Industry By-Products as Adsorbent Materials for Removing Fluoride and Arsenic from Drinking Water—A Review. *Appl. Sci.* **2022**, *12*, 3166. [CrossRef]

32. Illankoon, W.A.M.A.N.; Milanese, C.; Karunarathna, A.K.; Alahakoon, A.M.Y.W.; Rathnasiri, P.G.; Medina-Llamas, M.; Collivignarelli, M.C.; Sorlini, S. Development of a Dual-Chamber Pyrolizer for Biochar Production from Agricultural Waste in Sri Lanka. *Energies* **2023**, *16*, 1819. [CrossRef]
33. Illankoon, W.A.M.A.N.; Milanese, C.; Girella, A.; Medina-Llamas, M.; Magnani, G.; Pontiroli, D.; Ricco, M.; Collivignarelli, M.C. Sabrina Sorlini Biochar Derived from the rice industry by-products as sustainable energy storage material. In Proceedings of the 30th European Biomass Conference and Exhibition (EUBCE), Marseille, France, 9–12 May 2022; Chevet, P.-F., Scarlat, N., Grassi, A., Eds.; ETA-Florence Renewable Energies: Florence, Italy, 2022.
34. Tan, K.B.; Vakili, M.; Horri, B.A.; Poh, P.E.; Abdullah, A.Z.; Salamatinia, B. Adsorption of Dyes by Nanomaterials: Recent Developments and Adsorption Mechanisms. *Sep. Purif. Technol.* **2015**, *150*, 229–242. [CrossRef]
35. Illankoon, W.A.M.A.N.; Sorlini, S. Technical, Economical, and Environmental Comparison of Composting and Anaerobic Digestion of Organic Waste Fraction of Municipal Solid Waste in Sri Lanka. In *Waste-to-Resources 2021, Proceedings of the 9th International Symposium Circular Economy, MBT, MRF and Recycling, Karlsruhe, Germany, 18–20 May 2021*; Cuvillier Verlag: Göttingen, Germany, 2021.
36. Collivignarelli, M.C.; Caccamo, F.M.; Bellazzi, S.; Llamas, M.M.; Sorlini, S.; Milanese, C. Survey on Lombardy Region Wastewater Effluents and Application of Biochar from Biological Sewage Sludge for Wastewater Treatment. *Water* **2023**, *15*, 3636. [CrossRef]
37. Palansooriya, K.N.; Ok, Y.S.; Awad, Y.M.; Lee, S.S.; Sung, J.-K.; Koutsospyros, A.; Moon, D.H. Impacts of Biochar Application on Upland Agriculture: A Review. *J. Environ. Manag.* **2019**, *234*, 52–64. [CrossRef] [PubMed]
38. Wani, I.; Ramola, S.; Garg, A.; Kushvaha, V. Critical Review of Biochar Applications in Geoengineering Infrastructure: Moving beyond Agricultural and Environmental Perspectives. *Biomass Convers. Biorefinery* **2021**. [CrossRef]
39. Xu, G.; Lv, Y.; Sun, J.; Shao, H.; Wei, L. Recent Advances in Biochar Applications in Agricultural Soils: Benefits and Environmental Implications. *Clean (Weinh)* **2012**, *40*, 1093–1098. [CrossRef]
40. Illankoon, W.A.M.A.N.; Milanese, C.; Karunarathna, A.K.; Liyanage, K.D.H.E.; Alahakoon, A.M.Y.W.; Rathnasiri, P.G.; Collivignarelli, M.C.; Sorlini, S. Evaluating Sustainable Options for Valorization of Rice By-Products in Sri Lanka: An Approach for a Circular Business Model. *Agronomy* **2023**, *13*, 803. [CrossRef]
41. Zhou, Z.; Liu, Y.; Liu, S.; Liu, H.; Zeng, G.; Tan, X.; Yang, C.; Ding, Y.; Yan, Z.; Cai, X. Sorption Performance and Mechanisms of Arsenic(V) Removal by Magnetic Gelatin-Modified Biochar. *Chem. Eng. J.* **2017**, *314*, 223–231. [CrossRef]
42. Peng, P.; Lang, Y.-H.; Wang, X.-M. Adsorption Behavior and Mechanism of Pentachlorophenol on Reed Biochars: PH Effect, Pyrolysis Temperature, Hydrochloric Acid Treatment and Isotherms. *Ecol. Eng.* **2016**, *90*, 225–233. [CrossRef]
43. Mosleh, M.H.; Rajabi, H. NaOH-Benzoic Acid Modified Biochar for Enhanced Removal of Aromatic VOCs. *Sep. Purif. Technol.* **2024**, *330*, 125453. [CrossRef]
44. Rajapaksha, A.U.; Selvasembian, R.; Ashiq, A.; Gunarathne, V.; Ekanayake, A.; Perera, V.O.; Wijesekera, H.; Mia, S.; Ahmad, M.; Vithanage, M.; et al. A Systematic Review on Adsorptive Removal of Hexavalent Chromium from Aqueous Solutions: Recent Advances. *Sci. Total Environ.* **2022**, *809*, 152055. [CrossRef] [PubMed]
45. Ahmad, M.A.; Herawan, S.G.; Yusof, A.A. Equilibrium, Kinetics, and Thermodynamics of Remazol Brilliant Blue R Dye Adsorption onto Activated Carbon Prepared from Pinang Frond. *ISRN Mech. Eng.* **2014**, *2014*, 1–7. [CrossRef]
46. Rosales, E.; Meijide, J.; Pazos, M.; Sanromán, M.A. Challenges and Recent Advances in Biochar as Low-Cost Biosorbent: From Batch Assays to Continuous-Flow Systems. *Bioresour. Technol.* **2017**, *246*, 176–192. [CrossRef] [PubMed]
47. Jha, S.; Gaur, R.; Shahabuddin, S.; Tyagi, I. Biochar as Sustainable Alternative and Green Adsorbent for the Remediation of Noxious Pollutants: A Comprehensive Review. *Toxics* **2023**, *11*, 117. [CrossRef] [PubMed]
48. Pignatello, J.J. Interactions of Anthropogenic Organic Chemicals with Natural Organic Matter and Black Carbon in Environmental Particles. In *Biophysico-Chemical Processes of Anthropogenic Organic Compounds in Environmental Systems*; John Wiley & Sons, Inc.: Hoboken, NJ, USA, 2011; pp. 1–50.
49. Kılıç, M.; Keskin, M.E.; Mazlum, S.; Mazlum, N. Hg(II) and Pb(II) Adsorption on Activated Sludge Biomass: Effective Biosorption Mechanism. *Int. J. Miner. Process* **2008**, *87*, 1–8. [CrossRef]
50. Ambaye, T.G.; Vaccari, M.; van Hullebusch, E.D.; Amrane, A.; Rtimi, S. Mechanisms and Adsorption Capacities of Biochar for the Removal of Organic and Inorganic Pollutants from Industrial Wastewater. *Int. J. Environ. Sci. Technol.* **2021**, *18*, 3273–3294. [CrossRef]
51. Jeyasubramanian, K.; Thangagiri, B.; Sakthivel, A.; Dhaveethu Raja, J.; Seenivasan, S.; Vallinayagam, P.; Madhavan, D.; Malathi Devi, S.; Rathika, B. A Complete Review on Biochar: Production, Property, Multifaceted Applications, Interaction Mechanism and Computational Approach. *Fuel* **2021**, *292*, 120243. [CrossRef]
52. Ahmad, M.; Rajapaksha, A.U.; Lim, J.E.; Zhang, M.; Bolan, N.; Mohan, D.; Vithanage, M.; Lee, S.S.; Ok, Y.S. Biochar as a Sorbent for Contaminant Management in Soil and Water: A Review. *Chemosphere* **2014**, *99*, 19–33. [CrossRef]
53. Yang, G.-X.; Jiang, H. Amino Modification of Biochar for Enhanced Adsorption of Copper Ions from Synthetic Wastewater. *Water Res.* **2014**, *48*, 396–405. [CrossRef]
54. Liu, T.; Lawluvy, Y.; Shi, Y.; Ighalo, J.O.; He, Y.; Zhang, Y.; Yap, P.-S. Adsorption of Cadmium and Lead from Aqueous Solution Using Modified Biochar: A Review. *J. Environ. Chem. Eng.* **2022**, *10*, 106502. [CrossRef]
55. Tseng, R.-L. Mesopore Control of High Surface Area NaOH-Activated Carbon. *J. Colloid. Interface Sci.* **2006**, *303*, 494–502. [CrossRef] [PubMed]

56. Jang, H.M.; Yoo, S.; Choi, Y.-K.; Park, S.; Kan, E. Adsorption Isotherm, Kinetic Modeling and Mechanism of Tetracycline on Pinus Taeda-Derived Activated Biochar. *Bioresour. Technol.* **2018**, *259*, 24–31. [CrossRef]
57. Namazi, A.B.; Allen, D.G.; Jia, C.Q. Benefits of Microwave Heating Method in Production of Activated Carbon. *Can. J. Chem. Eng.* **2016**, *94*, 1262–1268. [CrossRef]
58. Liu, H.; Xu, G.; Li, G. Preparation of Porous Biochar Based on Pharmaceutical Sludge Activated by NaOH and Its Application in the Adsorption of Tetracycline. *J. Colloid. Interface Sci.* **2021**, *587*, 271–278. [CrossRef]
59. Friel, J.J. ASTM Standards in Microscopy. *Microscopy Today* **2005**, *13*, 40–43. [CrossRef]
60. Wijeyawardana, P.; Nanayakkara, N.; Gunasekara, C.; Karunarathna, A.; Law, D.; Pramanik, B.K. Removal of Cu, Pb and Zn from Stormwater Using an Industrially Manufactured Sawdust and Paddy Husk Derived Biochar. *Environ. Technol. Innov.* **2022**, *28*, 102640. [CrossRef]
61. Sykam, N.; Madhavi, V.; Rao, G.M. Rapid and Efficient Green Reduction of Graphene Oxide for Outstanding Supercapacitors and Dye Adsorption Applications. *J. Environ. Chem. Eng.* **2018**, *6*, 3223–3232. [CrossRef]
62. Sykam, N.; Jayram, N.D.; Rao, G.M. Highly Efficient Removal of Toxic Organic Dyes, Chemical Solvents and Oils by Mesoporous Exfoliated Graphite: Synthesis and Mechanism. *J. Water Process Eng.* **2018**, *25*, 128–137. [CrossRef]
63. Vayenas, C.; Brosda, S. Spillover-Modified Catalysis: Experimental Rules and Mathematical Modeling. *ChemInform* **2001**, *33*, 197–204.
64. Ye, W.; Pan, Y.; He, L.; Chen, B.; Liu, J.; Gao, J.; Wang, Y.; Yang, Y. Design with Modeling Techniques. In *Industrial Ventilation Design Guidebook*; Elsevier: Amsterdam, The Netherlands, 2021; pp. 109–183.
65. Sahu, O.; Singh, N. Significance of Bioadsorption Process on Textile Industry Wastewater. In *The Impact and Prospects of Green Chemistry for Textile Technology*; Elsevier: Amsterdam, The Netherlands, 2019; pp. 367–416.
66. Weber, T.W.; Chakravorti, R.K. Pore and Solid Diffusion Models for Fixed-Bed Adsorbers. *AIChE J.* **1974**, *20*, 228–238. [CrossRef]
67. Tran, H.N.; You, S.-J.; Hosseini-Bandegharaei, A.; Chao, H.-P. Mistakes and Inconsistencies Regarding Adsorption of Contaminants from Aqueous Solutions: A Critical Review. *Water Res.* **2017**, *120*, 88–116. [CrossRef]
68. Singh, A.K. Nanoparticle Ecotoxicology. In *Engineered Nanoparticles*; Elsevier: Amsterdam, The Netherlands, 2016; pp. 343–450.
69. Pal, P. Industry-Specific Water Treatment. In *Industrial Water Treatment Process Technology*; Elsevier: Amsterdam, The Netherlands, 2017; pp. 243–511.
70. Foo, K.Y.; Hameed, B.H. Insights into the Modeling of Adsorption Isotherm Systems. *Chem. Eng. J.* **2010**, *156*, 2–10. [CrossRef]
71. Kalam, S.; Abu-Khamsin, S.A.; Kamal, M.S.; Patil, S. Surfactant Adsorption Isotherms: A Review. *ACS Omega* **2021**, *6*, 32342–32348. [CrossRef] [PubMed]
72. Al-Ghouti, M.A.; Da'ana, D.A. Guidelines for the Use and Interpretation of Adsorption Isotherm Models: A Review. *J. Hazard. Mater.* **2020**, *393*, 122383. [CrossRef]
73. Shaaban, A.; Se, S.-M.; Mitan, N.M.M.; Dimin, M.F. Characterization of Biochar Derived from Rubber Wood Sawdust through Slow Pyrolysis on Surface Porosities and Functional Groups. *Procedia Eng.* **2013**, *68*, 365–371. [CrossRef]
74. Mor, S.; Manchanda, C.K.; Kansal, S.K.; Ravindra, K. Nanosilica Extraction from Processed Agricultural Residue Using Green Technology. *J. Clean. Prod.* **2017**, *143*, 1284–1290. [CrossRef]
75. Illankoon, W.A.M.A.N.; Milanese, C.; Girella, A.; Rathnasiri, P.G.; Sudesh, K.H.M.; Llamas, M.M.; Collivignarelli, M.C.; Sorlini, S. Agricultural Biomass-Based Power Generation Potential in Sri Lanka: A Techno-Economic Analysis. *Energies* **2022**, *15*, 8984. [CrossRef]
76. Xiao, B.; Sun, X.F.; Sun, R. Chemical, Structural, and Thermal Characterizations of Alkali-Soluble Lignins and Hemicelluloses, and Cellulose from Maize Stems, Rye Straw, and Rice Straw. *Polym. Degrad. Stab.* **2001**, *74*, 307–319. [CrossRef]
77. Sun, Y.; Webley, P.A. Preparation of Activated Carbons from Corncob with Large Specific Surface Area by a Variety of Chemical Activators and Their Application in Gas Storage. *Chem. Eng. J.* **2010**, *162*, 883–892. [CrossRef]
78. Azat, S.; Korobeinyk, A.V.; Moustakas, K.; Inglezakis, V.J. Sustainable Production of Pure Silica from Rice Husk Waste in Kazakhstan. *J. Clean. Prod.* **2019**, *217*, 352–359. [CrossRef]
79. Santana Costa, J.A.; Paranhos, C.M. Systematic Evaluation of Amorphous Silica Production from Rice Husk Ashes. *J. Clean. Prod.* **2018**, *192*, 688–697. [CrossRef]
80. Wang, Z.; Cao, J.; Wang, J. Pyrolytic Characteristics of Pine Wood in a Slowly Heating and Gas Sweeping Fixed-Bed Reactor. *J. Anal. Appl. Pyrolysis* **2009**, *84*, 179–184. [CrossRef]
81. Meléndez-Ortiz, H.I.; Perera-Mercado, Y.; Mercado-Silva, J.A.; Olivares-Maldonado, Y.; Castruita, G.; García-Cerda, L.A. Functionalization with Amine-Containing Organosilane of Mesoporous Silica MCM-41 and MCM-48 Obtained at Room Temperature. *Ceram. Int.* **2014**, *40*, 9701–9707. [CrossRef]
82. Umeda, J.; Kondoh, K. High-Purification of Amorphous Silica Originated from Rice Husks by Combination of Polysaccharide Hydrolysis and Metallic Impurities Removal. *Ind. Crops Prod.* **2010**, *32*, 539–544. [CrossRef]
83. Nandiyanto, A.B.D.; Oktiani, R.; Ragadhita, R. How to Read and Interpret FTIR Spectroscope of Organic Material. *Indones. J. Sci. Technol.* **2019**, *4*, 97. [CrossRef]
84. Islam, M.A.; Auta, M.; Kabir, G.; Hameed, B.H. A Thermogravimetric Analysis of the Combustion Kinetics of Karanja (*Pongamia pinnata*) Fruit Hulls Char. *Bioresour. Technol.* **2016**, *200*, 335–341. [CrossRef]
85. Suliman, W.; Harsh, J.B.; Abu-Lail, N.I.; Fortuna, A.-M.; Dallmeyer, I.; Garcia-Perez, M. Influence of Feedstock Source and Pyrolysis Temperature on Biochar Bulk and Surface Properties. *Biomass Bioenergy* **2016**, *84*, 37–48. [CrossRef]

86. Ahmad, M.; Lee, S.S.; Dou, X.; Mohan, D.; Sung, J.-K.; Yang, J.E.; Ok, Y.S. Effects of Pyrolysis Temperature on Soybean Stover- and Peanut Shell-Derived Biochar Properties and TCE Adsorption in Water. *Bioresour. Technol.* **2012**, *118*, 536–544. [CrossRef]
87. Windeatt, J.H.; Ross, A.B.; Williams, P.T.; Forster, P.M.; Nahil, M.A.; Singh, S. Characteristics of Biochars from Crop Residues: Potential for Carbon Sequestration and Soil Amendment. *J. Environ. Manag.* **2014**, *146*, 189–197. [CrossRef] [PubMed]
88. Enaime, G.; Baçaoui, A.; Yaacoubi, A.; Lübken, M. Biochar for Wastewater Treatment—Conversion Technologies and Applications. *Appl. Sci.* **2020**, *10*, 3492. [CrossRef]
89. Bai, S.; Tan, G.; Li, X.; Zhao, Q.; Meng, Y.; Wang, Y.; Zhang, Y.; Xiao, D. Pumpkin-Derived Porous Carbon for Supercapacitors with High Performance. *Chem. Asian J.* **2016**, *11*, 1828–1836. [CrossRef] [PubMed]
90. Ugwu, E.I.; Agunwamba, J.C. A Review on the Applicability of Activated Carbon Derived from Plant Biomass in Adsorption of Chromium, Copper, and Zinc from Industrial Wastewater. *Environ. Monit. Assess.* **2020**, *192*, 240. [CrossRef]
91. bin Jusoh, A.; Cheng, W.H.; Low, W.M.; Nora'aini, A.; Megat Mohd Noor, M.J. Study on the Removal of Iron and Manganese in Groundwater by Granular Activated Carbon. *Desalination* **2005**, *182*, 347–353. [CrossRef]
92. Sanz, J.; Lombrana, J.I.; De Luis, A.M.; Ortueta, M.; Varona, F. Microwave and Fenton's Reagent Oxidation of Wastewater. *Environ. Chem. Lett.* **2003**, *1*, 45–50. [CrossRef]
93. Dastgheib, S.A.; Rockstraw, D.A. A Model for the Adsorption of Single Metal Ion Solutes in Aqueous Solution onto Activated Carbon Produced from Pecan Shells. *Carbon. N. Y* **2002**, *40*, 1843–1851. [CrossRef]
94. Torres, J.; Pintos, V.; Gonzatto, L.; Domínguez, S.; Kremer, C.; Kremer, E. Selenium Chemical Speciation in Natural Waters: Protonation and Complexation Behavior of Selenite and Selenate in the Presence of Environmentally Relevant Cations. *Chem. Geol.* **2011**, *288*, 32–38. [CrossRef]
95. Yankovych, H.; Novoseltseva, V.; Kovalenko, O.; Marcin Behunova, D.; Kanuchova, M.; Vaclavikova, M.; Melnyk, I. New Perception of Zn(II) and Mn(II) Removal Mechanism on Sustainable Sunflower Biochar from Alkaline Batteries Contaminated Water. *J. Environ. Manag.* **2021**, *292*, 112757. [CrossRef]
96. Xu, Z.; Lin, Y.; Lin, Y.; Yang, D.; Zheng, H. Adsorption Behaviors of Paper Mill Sludge Biochar to Remove Cu, Zn and As in Wastewater. *Environ. Technol. Innov.* **2021**, *23*, 101616. [CrossRef]
97. Lian, W.; Li, H.; Yang, J.; Joseph, S.; Bian, R.; Liu, X.; Zheng, J.; Drosos, M.; Zhang, X.; Li, L.; et al. Influence of Pyrolysis Temperature on the Cadmium and Lead Removal Behavior of Biochar Derived from Oyster Shell Waste. *Bioresour. Technol. Rep.* **2021**, *15*, 100709. [CrossRef]
98. Zhao, S.; Ta, N.; Wang, X. Absorption of Cu(II) and Zn(II) from Aqueous Solutions onto Biochars Derived from Apple Tree Branches. *Energies* **2020**, *13*, 3498. [CrossRef]
99. Batool, M.; Khan, W.-D.; Hamid, Y.; Farooq, M.A.; Naeem, M.A.; Nadeem, F. Interaction of Pristine and Mineral Engineered Biochar with Microbial Community in Attenuating the Heavy Metals Toxicity: A Review. *Appl. Soil Ecol.* **2022**, *175*, 104444. [CrossRef]
100. Shen, Z.; Zhang, Y.; Jin, F.; McMillan, O.; Al-Tabbaa, A. Qualitative and Quantitative Characterisation of Adsorption Mechanisms of Lead on Four Biochars. *Sci. Total Environ.* **2017**, *609*, 1401–1410. [CrossRef] [PubMed]
101. Lian, F.; Xing, B. Black Carbon (Biochar) In Water/Soil Environments: Molecular Structure, Sorption, Stability, and Potential Risk. *Environ. Sci. Technol.* **2017**, *51*, 13517–13532. [CrossRef] [PubMed]
102. Mohan, D.; Sharma, R.; Singh, V.K.; Steele, P.; Pittman, C.U. Fluoride Removal from Water Using Bio-Char, a Green Waste, Low-Cost Adsorbent: Equilibrium Uptake and Sorption Dynamics Modeling. *Ind. Eng. Chem. Res.* **2012**, *51*, 900–914. [CrossRef]
103. Hussain, A.; Maitra, J.; Khan, K.A. Development of Biochar and Chitosan Blend for Heavy Metals Uptake from Synthetic and Industrial Wastewater. *Appl. Water Sci.* **2017**, *7*, 4525–4537. [CrossRef]